the observation that the Li atomic population hardly changes upon CO_2 coordination in $Li[Co(alcn)_2(CO)_2]$ (see Table II).

In conclusion, the presence of an alkali-metal cation is found to enhance the coordination of carbon dioxide by the electrostatic attractive interaction between Li^+ and CO_2 and the polarization of CO_2 by Li^+.

Acknowledgment. Calculations were carried out with an IBM 3081 instrument at the Centre de Calcul du CNRS in Strasbourg-Cronenbourg, except for some supplemental calculations carried out at the IMS Computer Center with support of a Grant-in-Aid for Scientific Research from the Japanese Ministry of Education, Science, and Culture (No. 60540306). We thank the staffs of the centers for their cooperation. S.S. is grateful to Drs. Benard, Demuynch, and Rohmer for helpful discussions and to the CNRS for financial support.

Registry No. $[Co(alcn)_2(CO_2)]^-$, 108663-10-1.

Contribution from the Christopher Ingold Laboratories, University College London, London, WC1H 0AJ, U.K., and Department of Medical Oncology, The University of Texas M. D. Anderson Hospital and Tumor Institute at Houston, Houston, Texas 77030

Neutral Chain Chloride- and Bromide-Bridged Platinum(II,IV) Complexes of 1,2-Diaminocyclohexane: Synthesis and Electronic, Infrared, Raman, and Resonance Raman Studies

Robin J. H. Clark,*† Vincent B. Croud,† and Abdul R. Khokhar‡

Received February 24, 1987

The synthesis and electronic, infrared, Raman, and resonance Raman spectra of the linear-chain complexes [Pt(*trans*-dach)X_2][Pt(*trans*-dach)X_4] (X = Cl, Br; dach = 1,2-diaminocyclohexane) are reported. The electronic spectra are characterized by broad, intense intervalence bands at ca. 25 000 cm^{-1} for X = Cl and ca. 18 200 cm^{-1} for X = Br. The temperature dependences of the infrared and resonance Raman spectra are discussed with particular reference to the Raman-active ν_1, $\nu_s(X-Pt^{IV}-X)$ mode and the role of unresolved components of this band in determining (a) the dependence on the exciting line of the ν_1 band wavenumber and (b) the excitation profile of ν_1.

Introduction

The complexes under study here, of stoichiometric formula Pt(*trans*-dach)X_3, where X = Cl or Br and dach = 1,2-diaminocyclohexane, were synthesized as part of continuing research into the antitumor activity of dihalo–amine complexes of platinum.[1-4] A X-ray study[5] of Pt(*trans*-dach)Cl_3 has indicated that the structure could be refined equally well in the space group *Pmnm* (centrosymmetric, with a disordered Cl^- above and below the $PtCl_2N_2$ plane) or in $Pmn2_1$ (noncentrosymmetric, 5-coordinate platinum(III)). The present spectroscopic study removes the ambiguity in favor of the former.

Additionally the temperature dependence of the Raman spectra, specifically the exciting-line dependence of the wavenumber of ν_1, $\nu_s(X-Pt^{IV}-X)$, and the form of its excitation profile are discussed in terms of relative intensity changes in unresolved components of ν_1.

Experimental Section

(i) Preparations. Materials. $K_2[PtCl_4]$ was purchased from Johnson Matthey, Seabrook, N.J., and 1,2-diaminocyclohexane, from Aldrich Chemical Co. *trans*-(+)-*S*,*S*-dach and *trans*-(−)-*R*,*R*-dach were purchased from Alfa Thiokol/Ventron Division, Danver, MA 01923.

Methods. Dihalo(1,2-diaminocyclohexane)platinum(II), sulfatoplatinum(II)–water, sulfato(*trans*-(+)-*S*,*S*)-1,2-diaminocyclohexane)platinum(II)–water, and sulfato(*trans*-(−)-(*R*,*R*)-1,2-diaminocyclohexane)platinum(II)–water were prepared by established methods.[4,6,7]

The (+)-*S*,*S*- and (−)-*R*,*R*-(*trans*-dach)PtX_3 complexes were synthesized by mixing stoichiometric quantities of the appropriate [Pt^{II}(*trans*-dach)(SO_4)] and [Pt^{IV}(*trans*-dach)$(SO_4)X_2$] in water, in the presence of excess of sodium halide.

Pt(*trans*-dach)Cl_3 was synthesized by adding [Pt(*trans*-dach)Cl_2], prepared from a racemic mixture of the trans amine, to concentrated HCl and heating for several hours.

All of the complexes were washed with acetone and diethyl ether and finally dried in vacuo.

Anal. Calcd for [Pt(*trans*-(+)-*S*,*S*-dach)Br_2][Pt(*trans*-(+)-*S*,*S*-dach)Br_4]: C, 13.11; H, 2.55; N, 5.10; Br, 43.71. Found: C, 13.63; H, 2.90; N, 5.25; Br, 42.33. Calcd for [Pt(*trans*-(−)-*R*,*R*-dach)Br_2][Pt(*trans*-(−)-*R*,*R*-dach)Br_4]: C, 13.11; H, 2.55; N, 5.10. Found: C, 13.64; H, 2.26; N, 5.02. Calcd for [Pt(*trans*-(+)-*S*,*S*-dach)Cl_2][Pt(*trans*-(+)-*S*,*S*-dach)Cl_4]: C, 17.32; H, 3.37; N, 6.73. Found: C, 17.53; H, 3.30; N, 6.69. Calcd for [Pt(*trans*-(−)-*R*,*R*-dach)Cl_2][Pt(*trans*-(−)-*R*,*R*-dach)Cl_4]: C, 17.32; H, 3.37; N, 6.73. Found: C, 17.14; H, 3.34; N, 6.45. Calcd for [Pt(dach)Cl_2][Pt(dach)Cl_4]: C, 17.32; H, 3.37; N, 6.73. Found: C, 17.24; H, 3.42; N, 6.61.

(ii) Instrumentation. Electronic spectra were recorded on a Cary 14 spectrometer at 295 K as Nujol mulls of the samples between quartz plates.

Infrared spectra were recorded in the region 650–20 cm^{-1}, as wax disks of the complexes, with a Bruker IFS 113V interferometer. An RIIC liquid-nitrogen cryostat was used to obtain spectra at ca. 80 K.

Raman spectra were recorded on a Spex 14018/R6 spectrometer. (RCA C 31034A photomultiplier). Exciting radiation was provided by Coherent Radiation Model CR 12 and CR 3000 K lasers. Samples were in the form of pressed disks, either of the pure complex or of a mixture with $K_2[SO_4]$. Raman spectra were recorded at ca. 40 K on an Air Products Displex Cryostat and at ca. 80 K with use of liquid nitrogen and a Dewar assembly. The usual technique for determining sample temperatures via Stokes/anti-Stokes ratios is invalid at resonance, and the use of a thermocouple would require that it be placed at the focal point of the laser beam on the crystal surface—a technical impossibility for Raman measurements. Thus, only nominal sample temperatures can be

† University College London.
‡ The University of Texas M. D. Anderson Hospital and Tumor Institute at Houston.

(1) Rosenberg, B.; Vancamp, L.; Trosko, J. E.; Mansour, V. H. *Nature (London)* **1969**, *222*, 385.
(2) Gale, G. R.; Walker, E. M.; Atkins, L. M.; Smith, A. B.; Mieschen, S. J. *Res. Commun. Chem. Pathol. Pharmacol.* **1974**, *7*, 529.
(3) Speer, R. J.; Ridgway, H.; Hill, J. H. *Wadley Med. Bull.* **1975**, *5*, 335.
(4) Speer, R. J.; Ridgway, H.; Hill, J. H. *J. Clin. Hematol. Oncol.* **1977**, *7*, 210.
(5) Gebreyes, K.; Zubieta, J. A., unpublished work. The data were collected on a crystal synthesized from the racemic mixture of the trans ligand ca. 0.02 × 0.12 × 0.25 mm at −113 ± 1 °C. The orthorhombic cell parameters, a = 9.312 (2), b = 10.396 (4), and c = 5.698 (3) Å, were refined in space group $Pmn2_1$. The Pt–Pt chain distance ($b/2$) is thus 5.198 Å; cf. that for [Pt(dach)$_2$][Pt(dach)$_2Cl_2$]Cl_4, which is 5.158 Å: Larsen, K. P.; Toftlund, H. *Acta Chem. Scand., Ser. A*, **1977**, *A31*, 182.
(6) Tobe, M. L.; Khokhar, A. R.; Braddock, B.; Ross, W. C. J.; Jones, M.; Connors, T. A. *Chem.-Biol. Interact.* **1972**, *5*, 415.
(7) Kidani, Y.; Noji, M.; Tsukagoshi, S.; Tashiro, T. *Gann* **1978**, *69*, 263.

0020-1669/87/1326-3284$01.50/0

Table I. Summary of the Data on the Complexes Studied

complex	color	intervalence max/cm^{-1} [a]	EP max/cm^{-1}	ω_1/cm^{-1} [f]	x_{11}/cm^{-1} [f]	$I(2\nu_1)/I(\nu_1)$ (λ_0/nm)	progn	dispersion of ν_1
[Pt(*trans*-dach)Cl$_2$]-[Pt(*trans*-dach)Cl$_4$]	yellow	~25 000	~21 500 [b]	314.9 ± 0.6	−1.5 ± 0.3	0.31 (476.2)	$7\nu_1$	
[Pt(*trans*-(−)-*R*,*R*-dach)Cl$_2$]-[Pt(*trans*-(−)-*R*,*R*-dach)Cl$_4$]	yellow	23 800		309.1 ± 0.3	−0.70 ± 0.05	0.70 (476.2)	$11\nu_1$	3 cm^{-1} (40 K) (red → 406.7 nm)
[Pt(*trans*-(+)-*S*,*S*-dach)Cl$_2$]-[Pt(*trans*-(+)-*S*,*S*-dach)Cl$_4$]	orange	23 800	20 000 [b]	309.4 ± 0.4	−0.73 ± 0.08	0.47 (476.2)	$11\nu_1$	
[Pt(*trans*-(−)-*R*,*R*-dach)Br$_2$]-[Pt(*trans*-(−)-*R*,*R*-dach)Br$_4$]	green metallic needles blue powder	18 200	~15 500 [c]	175.2 ± 0.2	−0.31 ± 0.2	0.68 (568.2)	$8\nu_1$	19.4 cm^{-1} (room temp) (752.5–457.9 nm) 14.6 cm^{-1} (40 K) (799.3–406.7 nm)
[Pt(*trans*-(+)-*S*,*S*-dach)Br$_2$]-[Pt(*trans*-(+)-*S*,*S*-dach)Br$_4$]	green metallic needles blue powder	18 200		175.3 ± 0.2 [d]	−0.43 ± 0.03 [d]	0.69 [d]	$5\nu_1$ [d]	
				176.3 ± 0.2 [e]	−0.50 ± 0.04 [e]	0.38 [e]	$7\nu_1$ [e]	

[a] By transmission as a Nujol mull at room temperature. [b] Recorded as a $K_2[SO_4]$ disk at ca. 50 K. [c] Recorded as a $K_2[SO_4]$ disk at ca. 40 K. [d] λ_0 = 568.2 nm, low power. [e] λ_0 = 568.2 nm, high power. [f] Calculated on the assumption that the most intense component of the ν_1 fundamental gives rise to the most intense component of the overtone.

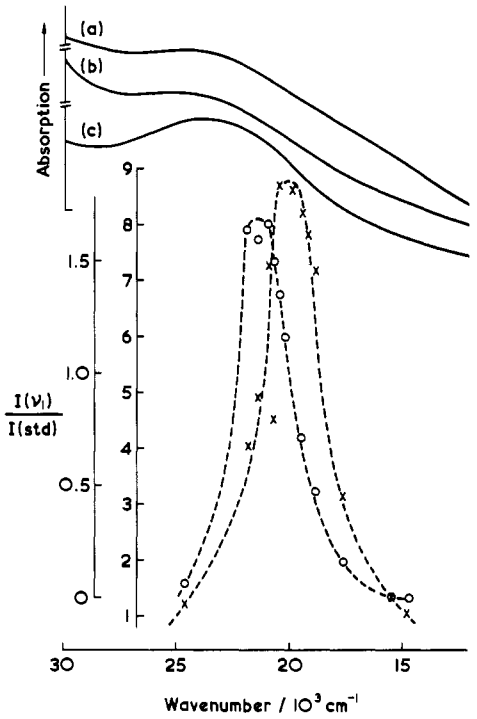

Figure 1. Electronic spectra (295 K) of (a) [Pt(*trans*-dach)Cl$_2$][Pt(*trans*-dach)Cl$_4$], (b) [Pt(*trans*-(−)-*R*,*R*-dach)Cl$_2$][Pt(*trans*-(−)-*R*,*R*-dach)Cl$_4$], and (c) [Pt(*trans*-(+)-*S*,*S*-dach)Cl$_2$][Pt(*trans*-(+)-*S*,*S*-dach)Cl$_4$], together with excitation profiles (80 K) of the ν_1 band of [Pt(*trans*-dach)Cl$_2$][Pt(*trans*-dach)Cl$_4$] (O) and [Pt(*trans*-(+)-*S*,*S*-dach)Cl$_2$][Pt(*trans*-(+)-*S*,*S*-dach)Cl$_4$] (×).

quoted. Spectra were calibrated by reference to the Rayleigh line. All Raman band intensities were corrected for the spectral response of the instruments.

Results and Discussion

Electronic Spectra. The colors of the crystals and powders, together with related spectroscopic data, are given in Table I. The transmission spectra of the chlorides (Figure 1) show a strong broad band in the violet region assigned to the $Pt^{II} \rightarrow Pt^{IV}$ intervalence charge-transfer transition. It occurs (by transmission measurements as Nujol mulls at room temperature) at ca. 23 800 cm^{-1} for the (−)-*R*,*R* and (+)-*S*,*S* complexes and at ca. 25 000 cm^{-1} for that made from the racemic mixture of ligands (the "mixed" complex). The latter is therefore predicted to have a weaker Pt^{II}/Pt^{IV} metal-center interaction compared with the former, i.e. a larger band gap. The relatively poor resolution of the intervalence band (Figure 1) is due to its close proximity to the cutoff caused by the Nujol at ca. 300 nm.

The broad, intense band assigned to the intervalence transition in the electronic spectra of the bromide-bridged complexes (Figure 2) occurs at ca. 18 200 cm^{-1} for both (+)-*S*,*S* and (−)-*R*,*R* complexes. In addition, both complexes have a weaker band at ca. 26 000 cm^{-1}, which is assigned to a d–d transition or a ligand-to-metal transition of the Pt^{IV} unit.

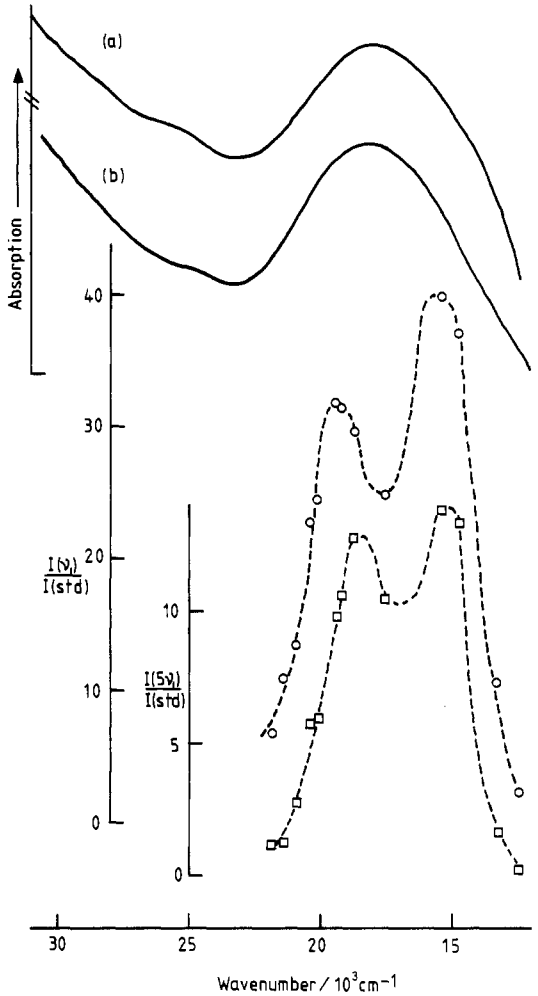

Figure 2. Electronic spectra (295 K) of (a) [Pt(*trans*-(+)-*S*,*S*-dach)Br$_2$][Pt(*trans*-(+)-*S*,*S*-dach)Br$_4$] and (b) [Pt(*trans*-(−)-*R*,*R*-dach)Br$_2$][Pt(*trans*-(−)-*R*,*R*-dach)Br$_4$] and excitation profiles (80 K) of the ν_1 (O) and $5\nu_1$ (□) bands of [Pt(*trans*-(−)-*R*,*R*-dach)Br$_2$][Pt(*trans*-(−)-*R*,*R*-dach)Br$_4$].

Infrared Spectra. The infrared spectra (Figures 3 and 4) have been recorded for all complexes at ca. 80 K and additionally at room temperature in the region 650–20 cm^{-1} for the "mixed" complex. The wavenumbers and assignments (based on those of related complexes)[8-10] of the bands are listed in Tables II and III.

(8) Berg, R. W.; Rasmussen, K. *Spectrochim. Acta* **1973**, *29A*, 319.

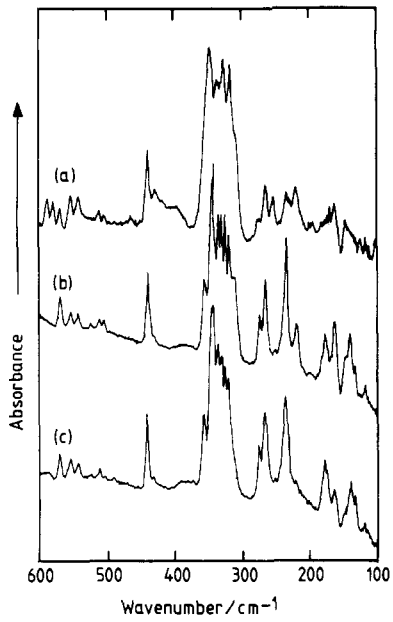

Figure 3. FTIR spectra (wax disks at 80 K) of (a) [Pt(*trans*-dach)Cl_2][Pt(*trans*-dach)Cl_4], (b) [Pt(*trans*-(−)-*R*,*R*-dach)Cl_2][Pt(*trans*-(−)-*R*,*R*-dach)Cl_4], and (c) [Pt(*trans*-(+)-*S*,*S*-dach)Cl_2][Pt(*trans*-(+)-*S*,*S*-dach)Cl_4].

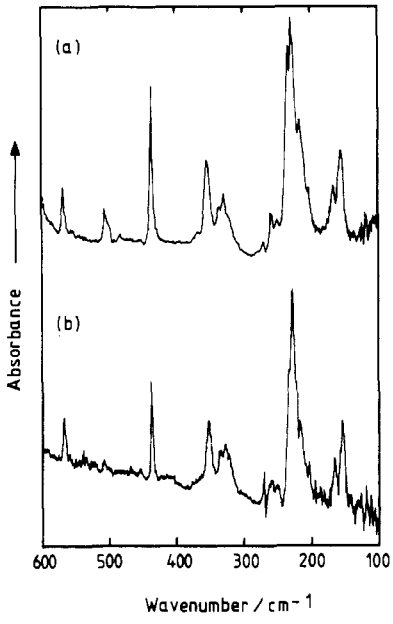

Figure 4. FTIR spectra (wax disks at 80 K) of (a) [Pt(*trans*-(+)-*S*,*S*-dach)Br_2][Pt(*trans*-(+)-*S*,*S*-dach)Br_4] and (b) [Pt(*trans*-(−)-*R*,*R*-dach)Br_2][Pt(*trans*-(−)-*R*,*R*-dach)Br_4].

The infrared spectra of the (−)-*R*,*R*- and (+)-*S*,*S*-(*trans*-dach)$PtCl_3$ complexes are virtually identical but differ slightly from that of the complex made from the racemic mixture (Figure 4). The main differences are in the ν(Pt–N) and ν(Pt–Cl) regions, with the wavenumbers of the bands being higher for the mixed complex than for the (−)-*R*,*R* and (+)-*SS* complexes (Table II). This could be due to the mixed complex having either a structure or symmetry slightly different from that of the (−)-*R*,*R* or (+)-*S*,*S* complexes. The slightly higher wavenumbers for the ν(Pt–Cl) bands suggests that the mixed complex has a weaker Pt^{II}/Pt^{IV} metal-center interaction than have the (−)-*R*,*R* or (+)-*S*,*S* complexes. If we compare the spectra of the mixed complex at ca. 80 K and room temperature (Table II), we can see that both the intensity and the wavenumbers of the ν(Pt–Cl) modes are very temperature sensitive. This may indicate the importance of these modes in determining the temperature dependence of the electronic properties of the complexes. Slight differences in temperature in recording the spectra of the (+)-*S*,*S* and (−)-*R*,*R* complexes may therefore explain the differences between the intensities of the ν(Pt–Cl) bands of these complexes (Table II). Alternatively, the differences may be due to chain length effects, different polycrystalline samples having different distributions of chain lengths.[11] Due to the presence of bands attributable to $\nu(Pt–Cl)_{eq}$,

Table II. Wavenumbers/cm^{-1} and Assignments of Bands Observed in the Infrared Spectra of (+)-*S*,*S*-, (−)-*R*,*R*-, and "Mixed"-(*trans*-dach)$PtCl_3$[a]

(+)-*S*,*S* (80 K)	(−)-*R*,*R* (80 K)	mixed (80 K)	mixed (room temp)	assignt
616 m	616 m	613 s	615 m	
		587 m	586 m	
		578 m	579 m	
569 w	568 w	568 m	570 m	
552 w	552 w	552 m		
541 w	541 w	540 m		ν(Pt–N)
		463 w	462 w	
440 sh	440 sh			
438 m	438 m	439 s	439 s	
435 sh	435 sh			
		427 s		
		396 m, br		
357 m	357 m			
354 m	354 m			
	348 sh	348 vs	350 vs	
344 s	344 s			
342 s	342 s		342 vs	ν(Pt–Cl) + ring modes
334 s	334 s	336 vs	336 vs	
330 s	330 s			
324 s	324 s	327 vs	326 vs	
314 w, sh	319 s	318 vs	316 vs	
	312 m	310 sh		
274 w	274 w	273 w	273 w	
264 m	265 m	264 m	262 m	δ(N–Pt–N)
250 w	250 w	253 m		
241 w, sh	241 w, sh			
234 s	234 s	231 m	231 m	
216 vw	218 w	220 m	218 m	δ(N–Pt–N)
176 w	176 w			
172 w	172 w			
162 w	162 m	162 m, br	162 m, br	$\delta(Cl–Pt^{IV}–Cl)$
146 sh	146 sh			
	140 w			
137 w	132 w			

[a] Recorded in the range 660–20 cm^{-1} as a wax disk. Bands below 130 cm^{-1} are very weak.

Table III. Wavenumbers/cm^{-1} and Assignments of Bands Observed in the Infrared Spectra of (−)-*R*,*R*- and (+)-*S*,*S*-(*trans*-dach)$PtBr_3$[a]

(−)-*R*,*R*	(+)-*S*,*S*	assignt
604 w	602 m	
	585 w	
567 m	567 m	
506 w	506 m	ν(Pt–N)
	500 w, sh	
	484 w	
436 s	436 s	
	368 w	
353 m	354 m	ring modes, δ(NCCN)
335 m	335 m	
328 m	328 m	
	271 w	δ(N–Pt–N)
258 m	258 m	
249 m	249 m	
232 s	234 vs	ν(Pt–Br)
226 vs[b]	227 vs[b]	
216 s	216 s	
	202 sh	
166 m	165 m	
154 m	154 m	

[a] Recorded in the range 660–20 cm^{-1} as a wax disk at ca. 80 K. Bands below 150 cm^{-1} are very weak. [b] May be ν_2, $\nu_{as}(Br–Pt^{IV}–Br)$.

(9) Watt, G. W.; Klett, D. S. *Inorg. Chem.* **1966**, *5*, 1128.
(10) Powell, D. B; Sheppard, N. *Spectrochim. Acta* **1961**, *17*, 68.

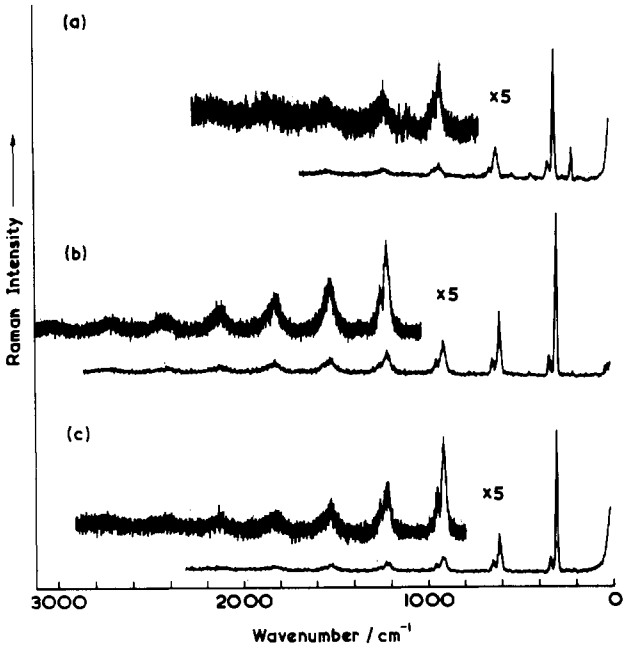

Figure 5. Resonance Raman spectra, as $K_2[SO_4]$ disks at ca. 50 K, with λ_0 = 476.2 nm (ca. 10-mW power at source), of (a) [Pt(*trans*-dach)Cl_2][Pt(*trans*-dach)Cl_4], (b) [Pt(*trans*-(−)-*R*,*R*-dach)Cl_2][Pt(*trans*-(−)-*R*,*R*-dach)Cl_4], and (c) [Pt(*trans*-(+)-*S*,*S*-dach)Cl_2][Pt(*trans*-(+)-*S*,*S*-dach)Cl_4], showing vibrational Raman spectra only.

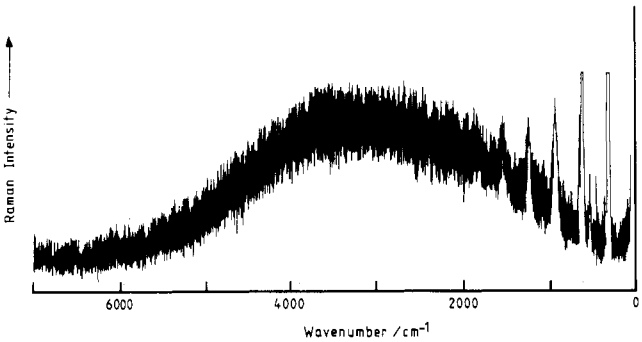

Figure 6. Resonance Raman spectrum of [Pt(*trans*-dach)Cl_2][Pt(*trans*-dach)Cl_4] as a $K_2[SO_4]$ disk at ca. 50 K, with λ_0 = 476.2 nm (ca. 10-mW power at source), showing the vibrational Raman spectrum together with luminescence band B.

it is not possible unambiguously to assign a band to ν_2, ν_{as}(Cl–Pt^{IV}–Cl) and hence to obtain, via its wavenumber drop on complex formation, a more accurate measure of the relative degree of metal-center interaction between the Pt^{II} and Pt^{IV} moieties.

Similarly, the spectra of the (+)-*S*,*S*- and (−)-*R*,*R*-(*trans*-dach)$PtBr_3$ complexes (Table III; Figure 4) are virtually identical, with weaker bands being observed in the (+)-*S*,*S*-(*trans*-dach)-$PtBr_3$ spectrum due to the disk's being more concentrated. Again, the only important differences between the spectra of the two complexes lie in the region assigned to ν(Pt–Br). It is not possible unambiguously to assign a band to the ν_2, ν_{as}(Br–Pt^{IV}–Br) vibration.

Resonance Raman Spectra. Chloride-Bridged Complexes. The Raman and resonance Raman spectra were recorded as $K_2[SO_4]$ disks at ca. 50 K with ca. 10-mW incident laser power; power much greater than this led to rapid sample decomposition, especially with violet excitation. The spectra of the complexes are shown in Figures 5–7, and the band wavenumbers and assignments are listed in Tables IV–VI.

The resonance Raman spectra of all three complexes are dominated by long overtone progressions in ν_1, the totally symmetric Cl–Pt^{IV}–Cl stretching mode. This is a feature characteristic

(11) Conradson, S. D.; Dallinger, R. F.; Swanson, B. I.; Croud, V. B.; Clark, R. J. H. *Chem. Phys. Lett.* **1987**, *135*, 463.

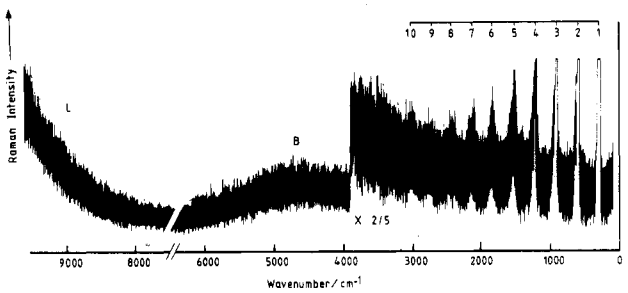

Figure 7. Resonance Raman spectrum of [Pt(*trans*-(−)-*R*,*R*-dach)Cl_2][Pt(*trans*-(−)-*R*,*R*-dach)Cl_4] as a solid disk at ca. 50 K, with λ_0 = 457.9 nm (ca. 10-mW power at source), showing the vibrational Raman spectrum together with luminescence bands L and B.

Table IV. Wavenumbers, Relative Intensities, Fwhm's, and Assignments of Bands Observed in the Resonance Raman Spectrum of [Pt(*trans*-dach)Cl_2][Pt(*trans*-dach)Cl_4][a]

$\tilde{\nu}$/cm^{-1}	$I(v_1\nu_1)/I(\nu_1)$	$\Delta\tilde{\nu}_{1/2}$/cm^{-1}	assignt
183.0			
216.8			δ(N–Pt–N)
220.8 sh			
312.5	1.0	12.0	ν_1, ν_s(Cl–Pt^{IV}–Cl)
344.3			ν(Pt–Cl)$_{eq}$
432.0			ring mode?
531.7			ν(Pt–N)
619.3	0.31	20	$2\nu_1$
654			ν_1 + ν(Pt–Cl)$_{eq}$
924.8	0.12	32	$3\nu_1$
962			$2\nu_1$ + ν(Pt–Cl)$_{eq}$
1232	<0.12	>32	$4\nu_1$
1273			$3\nu_1$ + ν(Pt–Cl)$_{eq}$
1540	<0.12	>32	$5\nu_1$
1855	<0.12	>32	$6\nu_1$
2155	<0.12	>32	$7\nu_1$

[a] Prepared from a racemic *trans*-dach mixture; spectrum recorded as a $K_2[SO_4]$ disk at ca. 50 K with λ_0 = 476.2 nm (ca. 10 mW).

Table V. Wavenumbers, Relative Intensities, Fwhm's, and Assignments of Bands Observed in the Resonance Raman Spectrum of [Pt(*trans*-(−)-*R*,*R*-dach)Cl_2][Pt(*trans*-(−)-*R*,*R*-dach)Cl_4][a]

$\tilde{\nu}$/cm^{-1}	$I(v_1\nu_1)/I(\nu_1)$	$\Delta\tilde{\nu}_{1/2}$/cm^{-1}	assignt
103			
167			δ(Cl–Pt^{IV}–Cl)
214.7			δ(N–Pt–N)
240.9			
251			
267			
307.7	1.00	10.8	ν_1, ν_s(Cl–Pt^{IV}–Cl)
330.4			ν(Pt–Cl)$_{eq}$
342.3			ν(Pt–Cl)$_{eq}$
525			ν(Pt–N)
614.7	0.7	19	$2\nu_1$
651			ν_1 + 342
918.8	0.38	26	$3\nu_1$
954			$2\nu_1$ + 342
1147.9			ω(NH_2)
1221.6	0.33	36	$4\nu_1$
1258			$3\nu_1$ + 342
1296			δ_t(H–C–H)?
1524	0.29	~50	$5\nu_1$
1559			$4\nu_1$ + 342
1825	<0.3	>50	$6\nu_1$
1875			
1973			
2127	<0.3	>50	$7\nu_1$
2175			
2423	<0.3	>50	$8\nu_1$
2493			
2720			$9\nu_1$
3015			$10\nu_1$
3292			$11\nu_1$

[a] Recorded as a $K_2[SO_4]$ disk at ca. 50 K with λ_0 = 476.2 nm (ca. 10 mW).

Table VI. Wavenumbers, Relative Intensities, Fwhm's, and Assignments of Bands Observed in the Resonance Raman Spectrum of [Pt(*trans*-(+)-*S,S*-dach)Cl_2][Pt(*trans*-(+)-*S,S*-dach)Cl_4][a]

$\tilde{\nu}$/cm^{-1}	$I(\upsilon_1\nu_1)/I(\nu_1)$	$\Delta\tilde{\nu}_{1/2}$/cm^{-1}	assignt
102			
168			δ(Cl–Pt^{IV}–Cl)
214.3			δ(N–Pt–N)
241.3			
250.9			
267			
307.7	1.00	10.6	ν_1, ν_s(Cl–Pt^{IV}–Cl)
330.2			ν(Pt–Cl)$_{eq}$
342.6			ν(Pt–Cl)$_{eq}$
525.7			ν(Pt–N)
614.7	0.47	19	$2\nu_1$
650.9			ν_1 + 342
920.7	0.25	28	$3\nu_1$
955.2			$2\nu_1$ + 342
1148			ω(NH_2)
1223.9	0.17	38	$4\nu_1$
1257.2			$3\nu_1$ + 342
1523.5	0.14	60	$5\nu_1$
1560.8			$4\nu_1$ + 342
1829	<0.14	>60	$6\nu_1$
1876			
2129	<0.14	>60	$7\nu_1$
2420	<0.14	>60	$8\nu_1$
2715	<0.14	>60	$9\nu_1$
3015	<0.14	>60	$10\nu_1$
3310			ν(NH_2)
3570			

[a] Recorded as a $K_2[SO_4]$ disk at ca. 50 K with λ_0 = 476.2 nm (ca. 10 mW).

of linear-chain mixed-valence complexes, and hence the (*trans*-dach)$PtCl_3$ complexes are certainly platinum(II,IV) chain rather than 5-coordinate platinum(III) species. The wavenumbers for ν_1 and hence $n\nu_1$ are virtually identical for the (+)-*S,S* and (−)-*R,R* complexes, the small differences being almost certainly due to different temperatures or chain length compositions of the samples, this causing changes in the relative intensities of unresolved components of the ν_1 band in each case. The wavenumber of ν_1 for the mixed complex is significantly higher than that of the (−)-*R,R* and (+)-*S,S* complexes, confirming that this complex has a weaker Pt^{II}/Pt^{IV} metal-center interaction than the (−)-*R,R* and (+)-*S,S* complexes. Other subsidiary progressions $\upsilon_1\nu_1 + \nu_n$ are observed, with ν_n being assigned to ν(Pt^{IV}–Cl)$_{eq}$ for all three complexes; this indicates that the ν(Pt^{IV}–Cl)$_{eq}$ modes are intimately coupled to the intervalence transition (see infrared section). This subsidiary progression is difficult to deconvolute from the higher overtones of ν_1. There are no peaks attributable to ν_1 or ν(Pt–Cl)$_{eq}$ of the (+)-*S,S* or (−)-*R,R* complexes in the spectra of the mixed complex, indicating that the percentage of (+)-*S,S* or (−)-*R,R* complex in the mixed complex is small or zero. Hence, neither the pure (−)-*R,R-trans*- or (+)-*S,S-trans*-dach complex is preferred when complexes are prepared from racemic dach mixtures. For the (−)-*R,R* complex both amino groups occupy equatorial positions on adjacent carbon atoms of the dach ring, and for the (+)-*S,S* both amino groups occupy axial positions. It would seem likely that, for the mixed complex, the geometry must have equatorial amino groups on one platinum center ((−)-*R,R*) and axial amino groups on the adjacent platinum atom ((+)-*S,S*), with the arrangement of alternating equatorial and axial configurations on the platinum centers continuing along the chain. Hence, the amines on adjacent platinum atoms in the mixed complex are not truly eclipsed, perhaps leading (for steric reasons) to slightly weaker metal-center interaction for the mixed complex compared with that for the pure (+)-*S,S* or (−)-*R,R* complexes as implied by the spectroscopic results.

The excitation profile (EP) of the (+)-*S,S* complex (Figure 1) maximizes at a wavenumber ca. 1500 cm^{-1} lower than that of the mixed complex (Figure 1), which is in agreement with the trend previously noted on the relative degree of Pt^{II}/Pt^{IV} interaction of the complexes. There may be a shoulder on the high-wavenumber side of the EP of the (+)-*S,S* complex. The reason for this will be discussed later.

Table VII. Wavenumbers, Relative Intensities, Fwhm's, and Assignments of Bands Observed in the Resonance Raman Spectrum of [Pt(*trans*-(+)-*S,S*-dach)Br_2][Pt(*trans*-(+)-*S,S*-dach)Br_4][a]

$\tilde{\nu}$/cm^{-1}	$I(\upsilon_1\nu_1)/I(\nu_1)$	$\Delta\tilde{\nu}_{1/2}$/cm^{-1}	assignt
174.2	1.0	5.6	ν_1, ν_s(Br–Pt^{IV}–Br)
206			δ(N–Pt–N) or ν(Pt–Br)$_{eq}$
233 w			ν(Pt–Br)$_{eq}$
267.6			ν(Pt–Br)$_{eq}$
348.5	0.69	12	$2\nu_1$
380			ν_1 + 206
520.8	0.51	20	$3\nu_1$
552			$2\nu_1$ + 206
692.8	~0.3	~25	$4\nu_1$
729			$3\nu_1$ + 206
863	<0.3	>25	$5\nu_1$

[a] Recorded as a $K_2[SO_4]$ disk at ca. 80 K; slits 200/250/200 μm; 568.2-nm excitation of <50 mW at the source.

Table VIII. Wavenumbers, Relative Intensities, Fwhm's, and Assignments of Bands Observed in the Resonance Raman Spectrum of [Pt(*trans*-(+)-*S,S*-dach)Br_2][Pt(*trans*-(+)-*S,S*-dach)Br_4][a]

$\tilde{\nu}$/cm^{-1}	$I(\upsilon_1\nu_1)/I(\nu_1)$	$\Delta\tilde{\nu}_{1/2}$/cm^{-1}	assignt
175.2[b]	1.0	7.2	ν_1, ν_s(Br–Pt^{IV}–Br)
206.2			δ(N–Pt–N) or ν(Pt–Br)$_{eq}$
234			ν(Pt–Br)$_{eq}$
349.7	0.38	12.6	$2\nu_1$
382			ν_1 + 206
408			ν_1 + ν(Pt–Br)$_{eq}$
454			
522.8	0.33	25	$3\nu_1$
556			$2\nu_1$ + 206
587			$2\nu_1$ + ν(Pt–Br)$_{eq}$
620			
628			ν_1 + 454?
695.4	0.16	32	$4\nu_1$
730			$3\nu_1$ + 206
866.9	0.05	39	$5\nu_1$
1040	<0.05	>39	$6\nu_1$
1203	<0.05	>39	$7\nu_1$

[a] Recorded as a $K_2[SO_4]$ disk at ca. 80 K; slits 200/250/200 μm; 568.2-nm excitation of ca. 100 mW. [b] ν_1 = 176.1 cm^{-1} for 514.5-nm excitation.

No dispersion of ν_1 with change in exciting line is observed for (−)-*R,R*-(*trans*-dach)$PtCl_3$ (at ca. 40 K) for exciting lines of wavelength greater than 457.9 nm (ν_1 being at ca. 310.6 cm^{-1}); for λ_0 = 406.7 nm excitation, however, ν_1 shifts to 313.1 cm^{-1}. For the same complex, the luminescence band B[12] (Figure 7) occurs for λ_0 at 476.5 nm at ca. 17 240 cm^{-1} absolute wavenumber. The luminescence band L[12] occurs at ≤11 500 cm^{-1} (Figure 7).

Bromide-Bridged Complexes. The Raman and resonance Raman spectra of (+)-*S,S*- and (−)-*R,R*-(*trans*-dach)$PtBr_3$ complexes were recorded at ca. 80 K as $K_2[SO_4]$ disks or at room temperature and at ca. 40 K as polycrystalline disks. These complexes are not as susceptible to decomposition by higher incident laser power as the chloride-bridged complexes.

The spectra of the complexes are shown in Figures 8 and 9 and the band wavenumbers and assignments are listed in Tables VII–IX.

The resonance Raman spectra are dominated by long overtone progressions in ν_1, the totally symmetric (Br–Pt^{IV}–Br) stretching vibration. The spectra of (+)-*S,S*-(*trans*-dach)$PtBr_3$ (Tables VII and VIII; Figure 8) indicate that the wavenumber of ν_1 as well as the intensity ratio $I(2\nu_1)/I(\nu_1)$ is dependent on the incident laser power. An 80-mW increase in laser power increases ν_1 by ca. 1 cm^{-1}. This could be due to a temperature-induced change in the band gap altering the position of the ν_1 dispersion curve (vide infra) or to temperature-induced changes in the relative intensities of unresolved components of ν_1 (in this case a selective increase in

(12) Tanino, H.; Kobayashi, K. *J. Phys. Soc. Jpn.* **1983**, *52*, 1446.

Table IX. Wavenumbers, Relative Intensities, Fwhm's, and Assignments of Bands Observed in the Resonance Raman Spectrum of [Pt(*trans*-(−)-*R*,*R*-dach)Br_2][Pt(*trans*-(−)-*R*,*R*-dach)Br_4][a]

$\tilde{\nu}$/cm^{-1}	$I(v_1\nu_1)/I(\nu_1)$	$\Delta\tilde{\nu}_{1/2}$/cm^{-1}	assignt
69			} plasma?
116			
174.4	1.0	5.6	ν_1, ν_s(Br–Pt^{IV}–Br)
206.3			δ(N–Pt–N) or ν(Pt–Br)$_{eq}$
214			} ν(Pt–Br)$_{eq}$
235			
348.9	0.68	13.6	$2\nu_1$
381.7			ν_1 + 206
406			ν_1 + 235
455			δ(NCCN)?
522.2	0.41	18	$3\nu_1$
556			$2\nu_1$ + 206
582			$2\nu_1$ + 235
608			
694.4	0.31	30	$4\nu_1$
728			$3\nu_1$ + 235
777			ν_1 + 608?
868.5	0.20	38	$5\nu_1$
947			$2\nu_1$ + 608?
1037	0.15	44	$6\nu_1$
1209	<0.15	>44	$7\nu_1$
1379	<0.15	<44	$8\nu_1$

[a] Recorded as a $K_2[SO_4]$ disk at ca. 80 K; slits 200/250/200 μm; 568.2-nm excitation.

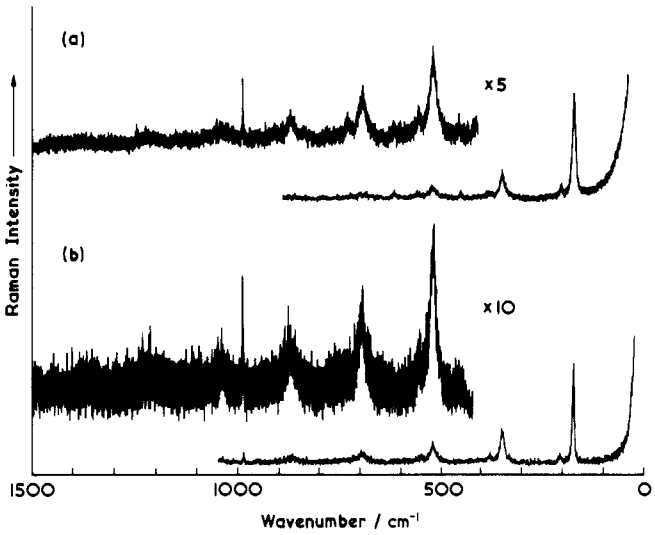

Figure 8. Resonance Raman spectra of [Pt(*trans*-(+)-*S*,*S*-dach)Br_2]-[Pt(*trans*-(+)-*S*,*S*-dach)Br_4] as $K_2[SO_4]$ disks at ca. 80 K, with λ_0 = 568.2 nm: (a) ca. 100-mW power at source; (b) ca. 20 mW power at source.

intensity of the higher wavenumber components). Except for temperature effects, however, the spectra of (−)-*R*,*R* and (+)-*S*,*S*-(*trans*-dach)$PtBr_3$ are identical, as expected.

Subsidiary progressions, $v_1\nu_1 + \nu_n$, where ν_n is assigned to ν-(Pt–Br)$_{eq}$, are observed. This involvement of ν(Pt–X)$_{eq}$ in the resonance Raman spectrum is identical with that observed in the (*trans*-dach)$PtCl_3$ complexes.

It is interesting that, in the spectra of (+)-*S*,*S*-(*trans*-dach)-$PtBr_3$, the intensity of the subsidiary progressions relative to $n\nu_1$ seems to be dependent on the incident laser power, and hence on the temperature. It has already been noted that, in the infrared spectra of the (*trans*-dach)PtX_3 complexes, the intensities of the ν(Pt–X) bands appear to be very temperature sensitive. This can be shown,[11] at least for the Raman-active $n\nu_1$ bands, to be due to relative intensity changes of unresolved components of $n\nu_1$ with temperature.

The EP maximum, which occurs at or near the absorption edge, is at ca. 15 500 cm^{-1} for the ν_1 band of the (−)-*R*,*R*-(*trans*-dach)$PtBr_3$ complex as a $K_2[SO_4]$ disk at ca. 40 K (Figure 2). There is a second, weaker, maximum at ca. 19 500 cm^{-1}. This

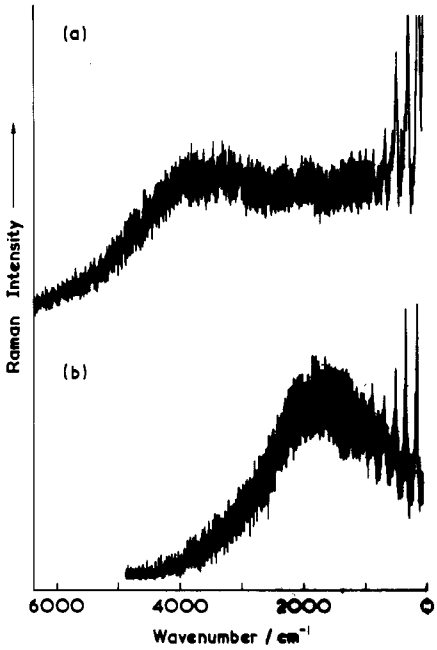

Figure 9. Resonance Raman spectra of [Pt(*trans*-(−)-*R*,*R*-dach)Br_2]-[Pt(*trans*-(−)-*R*,*R*-dach)Br_4] as $K_2[SO_4]$ disks at ca. 80 K,showing vibrational Raman spectra together with luminescence band B: (a) λ_0 = 468.1 nm; (b) λ_0 = 520.8 nm.

Table X. Wavenumbers of the ν_1 Band of [Pt(*trans*-(−)-*R*,*R*-dach)Br_2][Pt(*trans*-(−)-*R*,*R*-dach)Br_4], Measured at the Peak Maximum with Different Exciting Lines[a]

at ca. 40 K		at room temp	
λ_0/nm	ν_1/cm^{-1}	λ_0/nm	ν_1/cm^{-1}
406.74	187.3		
457.94	177.4	457.94	193.0 or 171.1
476.49	177.0	476.49	177.4
487.99	176.4	487.99	176.3
496.51	176.0	501.72	176.6
514.53	175.5	514.53	176.1
530.87	175.5	530.87	176.2
568.20	174.1	568.19	175.6
647.10	171.9	647.10	173.7, 173.0
676.46	172.9	676.46	173.4, 172.6
752.55	173.1[b]	752.55	173.6, 172.0
799.32	172.7[c]		

[a] Recorded as solid disks; slits 190/250/190 μm; cylindrical lens to line focus the beam; maxima accurate to ±0.3 cm^{-1}. [b] A band is also present at 164.1 ± 0.4 cm^{-1}. [c] A band is also present at 160.8 ± 0.5 cm^{-1}.

and the shoulder in the EP of (+)-*S*,*S*-(*trans*-dach)$PtCl_3$ are caused by unresolved components of ν_1. The components have been shown[11] to have different EP maxima, with the components of high wavenumber maximizing further to the blue than those of low wavenumber; the maxima occur sequentially depending on the component band wavenumber. The absolute intensification of the components increases as the wavenumber of the components decreases. Hence asymmetric EP's are obtained for polycrystalline samples, the asymmetry being toward the blue, with occasional partial resolution of the component EP's giving rise to shoulders or second maxima. The excitation profile of the $5\nu_1$ band also has two maxima, which occur at ca. 800 cm^{-1} lower than the corresponding peaks of the ν_1 excitation profile. If both sets of data are plotted against scattered rather than incident photon wavenumber, then the maxima of the excitation profiles of the ν_1 and $5\nu_1$ bands are virtually coincident. This is to be expected if intensity enhancement of the resonant mode(s) occurs when either the incident or scattered radiation is of wavenumber near or at that of the resonant electronic transition.[13]

(13) Loudon, R. *Proc. R. Soc., London, A* **1963**, *275*, 218.

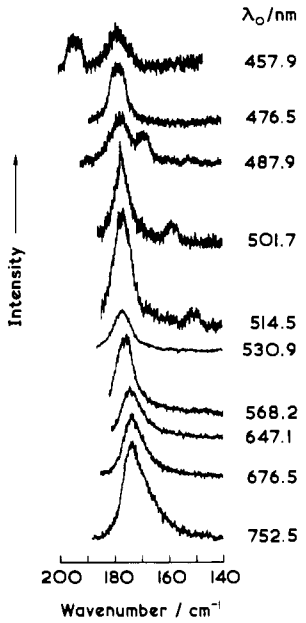

Figure 10. The ν_1 band of [Pt(*trans*-(−)-*R*,*R*-dach)Br_2][Pt(*trans*-(−)-*R*,*R*-dach)Br_4] recorded as a solid disk at room temperature for exciting lines in the range 457.9–752.5 nm.

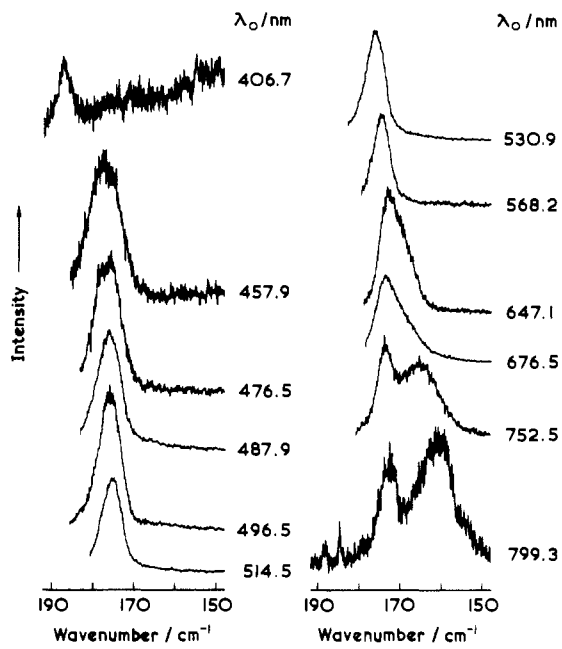

Figure 11. The ν_1 band of [Pt(*trans*-(−)-*R*,*R*-dach)Br_2][Pt(*trans*-(−)-*R*,*R*-dach)Br_4] recorded as a solid disk at ca. 40 K for exciting lines in the range 406.7–799.3 nm.

The dispersion of ν_1 with change in ν_0 has been measured for (−)-*R*,*R*-(*trans*-dach)$PtBr_3$, as a polycrystalline disk at ca. 40 K and room temperature (Figures 10 and 11; Table X). The form of the dispersion curve is the same as predicted previously.[14] However, it is now known that most of the dispersion can be explained in terms of different component bands of ν_1 changing in relative intensities with changing ν_0, the lowest wavenumber components maximizing in intensity in the red and the highest in the blue. There is no appreciable dispersion in ν_1 for exciting lines less than the band gap, E_g.[14] For ν_0 of energy just greater than E_g, the ν_1 band maximum has a weak dependence on ν_0, and for ν_0 much greater than E_g there is a strong dependence. This is because the wavenumber separation between the unresolved components increases with increasing wavenumber of the component, and the higher the wavenumber of the component, the further to the blue is the resonance position (i.e. the further away from E_g). If we compare the ν_1 value for λ_0 = 457.9 nm at 40 K with that at room temperature, we see that the latter is the greater. This implies that this ν_0 is much more above E_g at room temperature than at 40 K; i.e., the band gap is narrower at room temperature than at 40 K. This conclusion is in agreement with the data obtained for the temperature dependence of the electronic spectra[15] and excitation profiles.[16] It should be noted that the ν_1 band, with different exciting lines, is rarely symmetric owing to the presence of unresolved components. The ν_1 band is slightly asymmetric to the low-wavenumber side for $\nu_0 < E_g$ but asymmetric to the high-wavenumber side for $\nu_0 > E_g$. It is obvious that the dispersion of ν_1 with ν_0 can be used as a crude method of locating the band gap in these mixed-valence halogen-bridged complexes but that it is a much less accurate method than is EP analysis.

No luminescence band L could be located for the bromide-bridged complexes, the maximum being expected to occur beyond the range of detection of the spectrometer (i.e. <12 000 cm^{-1}). The ν_0-dependent band B was, however, apparent and is shown in Figure 10 for the (−)-*R*,*R*-(*trans*-dach)$PtBr_3$ complex.

Conclusion

The spectroscopic evidence indicates that the (*trans*-dach)PtX_3 complexes are mixed-valence Pt^{II}/Pt^{IV} species and not 5-coordinate platinum(III) complexes and thus that they can be formulated as [Pt^{II}(*trans*-dach)X_2][Pt^{IV}(*trans*-dach)X_4]. It has been shown that the wavenumber and intensity of the Pt–X modes are temperature sensitive and that the resonance Raman spectra, EP's and ν_1 dispersion can be explained in terms of the presence of components of ν_1 that are both temperature- and ν_0-sensitive in terms of their relative intensities.

Acknowledgment. This work was supported by the SERC (V.B.C.) and by the National Cancer Institute (Grant CA 41581 to A.R.K.).

(14) Clark, R. J. H.; Croud, V. B. *J. Phys. C* **1986**, *19*, 3467.
(15) Tanaka, M.; Kurita, S.; Kojima, T.; Yamada, Y. *Chem. Phys.* **1984**, *91*, 257.
(16) Croud, V. B. Ph.D. Thesis, University of London, 1986.